Mathematical Biosciences 392 (2026) 109601

Contents lists available at ScienceDirect

Mathematical Biosciences

journal homepage: www.elsevier.com/locate/mbs

How human behavior drives the balance of symptomatic and asymptomatic cases in emerging infections

Asma Azizi [a,*], Zhuolin Qu [b], Caner Kazanci [c,d]

[a] Department of Mathematics, Kennesaw State University, 30060, Marietta, GA, USA
[b] Department of Mathematics, University of Texas at San Antonio, San Antonio, 78249, TX, USA
[c] Department of Mathematics, University of Georgia, 30602, Athens, GA, USA
[d] College of Engineering, University of Georgia, 30602, Athens, GA, USA

ARTICLE INFO

Keywords:
Human behavior
Social distancing
Symptomatic and asymptomatic strains
Mathematical modeling

ABSTRACT

Human behavioral changes in response to observing disease in others play a crucial role in the spread of epidemics. These behaviors create selective pressures that influence a virus's ability to survive. This study explores how human behavioral adaptations influence the co-evolution of symptomatic and asymptomatic pathogen strains during an epidemic. Using a deterministic Susceptible-Infectious-Removed (SIR) model, it examines the role of spontaneous social distancing (SD) in shaping the selection pressures on these strains. The analysis highlights how behavioral changes can drive shifts in the prevalence of symptomatic versus asymptomatic cases, offering insights into the evolutionary dynamics of pathogen variants. Individuals initiate SD after contact with symptomatic cases, either by reducing interactions with everyone or by specifically avoiding symptomatic individuals. The analysis shows that homogeneous contact reduction tends to favor symptomatic strain, while targeted avoidance of symptomatic cases promotes the selection of asymptomatic one. The study underscores the complex, non-linear dynamics of selections under different levels of social distancing. A global sensitivity analysis highlights the significance of behavioral parameters in controlling the overall size of the infection. The findings emphasize the need for public health strategies that account for human behavior to effectively limit the spread and evolution of viral strains.

1. Introduction

During outbreaks of infectious diseases, individuals often undergo various behavioral changes to protect themselves and others from the spread of the disease. These behavioral changes are highly complex, depending on factors such as information or misinformation sources [1,2], perceived risks linked to behavioral modifications, such as fear [3–5], government-mandated rules like lockdown, and social pressures, such as peer influence [6]. This perspective has coalesced into the field of *behavioral epidemiology of infectious diseases* [7], which examines how individual and collective responses shape transmission and control across epidemics. Foundational reviews synthesize mechanisms and evidence spanning risk perception, information flow, social influence, and policy context [8–11].

A wide range of models has explored how awareness and behavioral adaptation influence infection spread and control [12–20]. These studies range from compartmental ODE models [17,21,22] to individual-based network models [23–26], focusing on specific infections such as influenza and COVID-19 [18,27,28] as well as generic epidemic processes [16,17,19,20,29]. Beyond distancing-focused responses, a substantial literature has examined vaccination behavior, refusal, and hesitancy as behavioral determinants of epidemic dynamics [30–32], underscoring that behavior can modify both contact patterns and per-contact risk. These models collectively show that while timely behavioral adaptation can temporarily reduce prevalence, it does not necessarily minimize the total epidemic size. This occurs because a decrease in incidence may reduce individuals' motivation to maintain protective measures.

One recurring challenge in emerging and re-emerging infections is pathogen evolution. The initially circulating lineage in humans (i.e., an early or ancestral strain) is often relatively poorly adapted and exhibits lower effective transmissibility [33]. As transmission continues, new lineages may arise with enhanced transmissibility. This evolutionary process can also alter the clinical profile of infection, sometimes shifting the proportion of symptomatic versus asymptomatic cases. For example, relative to Alpha (B.1.1.7), the Delta variant (B.1.617.2) of COVID-19 was associated with a higher likelihood of symptomatic and severe infections [34] and a substantially higher risk of hospital admission (e.g., adjusted hazard ratio ≈ 2.32, 95% CI 1.29–4.16, in UK

* Corresponding author.
E-mail address: aazizi@kennesaw.edu (A. Azizi).

https://doi.org/10.1016/j.mbs.2025.109601
Received 17 July 2025; Received in revised form 16 November 2025; Accepted 14 December 2025
Available online 24 December 2025

data) and increased emergency-care attendance [35,36]. By contrast, Omicron (B.1.1.529) combined higher transmissibility with markedly lower severity than Delta [37]: large UK analyses estimated a 45–75% lower risk of hospital admission overall, with age-specific adjusted HRs in the range $\sim 0.25 - -0.55$, and similar reductions for severe outcomes [38–40]. Comparative reports also note Omicron's greater reproduction number relative to prior variants [39].) The study of *competing viral strains* has a deep foundation dating back to the 1990s, with multi-strain theory developed for influenza and other pathogens [41,42] and broader evolutionary–epidemiological treatments [43]. Subsequent work examined how population structure and contact patterns shape replacement or coexistence [44] and how antigenic and clinical differences map into fitness [28]. During COVID-19, this framework was extensively applied to quantify the transmissibility and replacement dynamics of variants of concern [45–48].

Environmental changes, including shifts in population density [49], behavioral changes, or public health interventions [43,44,50], have been linked to the emergence of new variants that differ in the proportion of symptomatic versus asymptomatic cases. As a result, human behavioral adaptations, while not directly, can indirectly influence the selective pressures on symptomatic and asymptomatic strains of the virus [51]. Mathematical modeling of infectious diseases is a core pillar of public health practice, informing surveillance, forecasting, resource allocation, and policy-e.g., estimating reproduction numbers, projecting healthcare demand, evaluating intervention trade-offs, and comparing intervention strategies. It has underpinned responses to, including but not limited to, influenza [52–54], dengue fever [55,56], and HIV [57]. However, the relationship between human behavior and pathogen strain selection deserves more attention. In particular, the minimal decomposition of transmission rate into contact frequency and per-contact transmissibility-standard in empirical contact studies [58,59]-provides a transparent lens to study how behavior shifts selection between strains with different clinical profiles. Given this context, the central question guiding our research is as follows: *How do alterations in human behavior influence the selection of symptomatic and asymptomatic strains of a pathogen?*

This paper explores the influence of human behavioral changes on the co-evolution of the resident (symptomatic) and the emerging (asymptomatic) versions of one variant of a virus. These strains exhibit differences in their initial fitness, impacting individual behaviors and potentially conferring a selective advantage to one of them. Using the standard Susceptible-Infectious-Removed (SIR) model, we investigate how individuals' adaptation to the outbreak, reflected in behavioral changes, affects the co-dynamics of these two viral strains. Various aspects of human behavior contribute to behavioral changes, such as relational exchange (e.g., replacing sick individuals with healthy ones in the workplace) [60], personal hygiene practices [61], voluntary vaccination, and vaccination compliance [62]. Additionally, distinguishing between "risky" and "careful" individual behaviors [13,24,51,63,64], as well as the concept of Social Distancing (SD), plays a role. In our context, behavior change refers specifically to one form of spontaneous SD-voluntary adjustments to contact patterns in response to perceived risk-following the convention of Poletti et al. [20]; This contrasts with enforced (mandated) distancing policies. That is, for simplicity, factors such as social psychology and policy changes are not considered. Spontaneous SD involves individuals choosing to reduce their contacts when they perceive a risk of infection, such as when they encounter a symptomatic infected person. We will use SD and behavioral change interchangeably in this context. Accordingly, we position our contribution at the interface of behavioral epidemiology and competing-strain dynamics: we analyze how spontaneous behavioral responses that modify contact patterns shift selection between symptomatic and asymptomatic strains. While our main focus is on contact-based responses, and we situate our findings alongside established behavioral mechanisms (awareness contagion and vaccination behavior) synthesized in prior reviews [7–11,30–32].

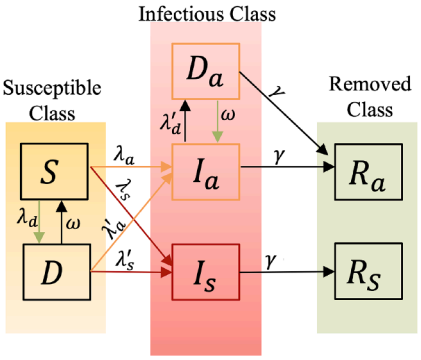

Fig. 1. Schematic of the Model Eq. (7). Compartments are represented by geometric shapes: Susceptible classes are represented by black boxes in the yellow-shaded area, infectious classes are depicted in red/orange boxes within the red-shaded area, and removed classes are displayed in black within the green-shaded area. Arrows indicate the flow between compartments, with orange and red arrows representing infection transmission, and green arrows indicating behavior change.

2. Method

We modeled a closed population of N individuals, divided into three primary classes: Susceptible, Infectious, and Removed.

The susceptible class comprises two groups: normal susceptible individuals (S) with an average contact rate of c, and altered susceptible individuals (D), who have adopted distancing behavior (here, D denotes distanced) and therefore reduce their contacts to lower their exposure risk.

The infectious class consists of three groups: Asymptomatically infected individuals (I_a), who exhibit no symptoms and behave similarly to normal susceptible individuals with a contact rate c. Individuals in class D_a are asymptomatic individuals who reduce their contact for self-protection. Finally, I_s denotes the symptomatically infected class, with an average contact rate c_s (usually $\leq c$). Individuals in this class show symptoms, triggering behavioral changes in susceptible and asymptomatic infected individuals.

The removed classes R_a and R_s include individuals who have recovered from asymptomatic and symptomatic infections, respectively, and those who have died due to disease-related mortality.

These individuals interact, contributing to the spread of infection and behavioral changes through a Susceptible-Infected-Recovered (SIR) structure. The overall structure of the model is illustrated in Fig. 1, while all state variables and parameters are summarized in Table 1, and the model is described in detail in the following subsections.

In this work, we focus on behavioral change expressed through altered contact patterns in the D and D_a groups. Individuals who adopt distancing reduce their overall contact rate from c to $(1-\sigma)c$, $\sigma \in [0,1]$, and may additionally practice targeted avoidance of symptomatic individuals, reducing the number of contacts involving I_s from c_s to $(1-\alpha)c_s$, $\alpha \in [0,1]$. These behavioral modifications determine how contact volume and mixing patterns are reshaped in response to symptom visibility.

Behavioral responses may also act by reducing the per-contact transmission probability (e.g., through improved hygiene, masking, or other precautionary actions). Because such mechanisms modify infectiousness rather than contact patterns, they alter the force of infection differently from the distancing behaviors modeled here. To contrast these behavioral pathways, we include a brief additional analysis in the Supplementary Material (Section S2), where transmission probabilities are reduced while contact rates are held fixed for the altered cohorts.

Table 1
Model variables and parameters, notations, descriptions, and units.

		Description	Unit
State Variables	S	Size of susceptible individuals	human
	D	Size of altered susceptible individuals	human
	I_a	Size of asymptomatically infected individuals	human
	D_a	Size of altered asymptomatically infected individuals	human
	I_s	Size of symptomatically infected individuals	human
	R_a	Size of asymptomatic recovered individuals	human
	R_s	Size of symptomatic recovered or dead individuals	human
	N	Population size	human
Epidemiological Parameters	β_s	Per contact prob. of trans. for symp. infected individuals	1/contact
	β_a	Per contact prob. of trans. for asymp. infected individuals	1/contact
	c_s	Number of contacts per day for symp. cases	contact/day
	c	Number of contacts per day for susceptibles and asymp. individuals	contact/day
	γ	Recovery rate	1/day
Behavioral Change Parameters	q	Fraction of susceptible and asymptomatic infected individuals who practice SD upon contact with symptomatic infected individuals	1
	ω	SD waning rate	1/day
	σ	Contact reduction level for D and D_a individuals: fraction of contacts reduced with all individuals	1
	α	Contact avoidance level for D and D_a individuals: fraction of contacts reduced with symptomatic individuals	1

2.1. Infection spreading

In our model, transmission preserves the phenotype of the infecting variant: infections caused by the symptomatic (I_s) and asymptomatic (I_a) strains remain symptomatic or asymptomatic, respectively. This assumption reflects two phenotypic manifestations of the same pathogen rather than two independent pathogens, with one strain always producing symptomatic cases and the other always causing asymptomatic cases.

S → I_s transition. Individuals in class S may move to class I_s after an infectious contact with the symptomatic individuals, I_s. The force of infection for the symptomatic strain is given by

$$\lambda_s = c\beta_s \frac{c_s I_s}{C_t}, \quad C_t = c(S + I_a + R) + (1-\sigma)c(D + D_a) + c_s I_s, \tag{1}$$

which depends on the number of contacts S an individual has per unit time, c, the probability of transmission for the symptomatic strain per contact, β_s, and the likelihood of having contact with I_s individuals, $c_s I_s/C_t$. Here, the term C_t is defined as the total *effective* contacts for all classes: c is the contact rate for normally behaved individuals in S, I_a, and R ($= R_s + R_a$) classes, $\sigma \in (0, 1]$ is the fraction of reduction in contacts for altered individuals in classes D and D_a (and $1-\sigma$ represents the remaining fraction that accounts for effective contacts), and c_s is the contact rate for symptomatic individuals in class I_s. This formulation follows the preferential mixing framework, which generalizes the classical proportionate mixing assumption [65–67]. In the classical case, all individuals have the same contact rate, and contact probabilities are proportional to group size. Here, since contact rates differ among groups-normal (c), altered ($(1-\sigma)c$), and symptomatic (c_s)-the frequency of contacts is weighted by group-specific contact rate while maintaining symmetric mixing between the groups. The denominator C_t, thus, represents the total *effective* number of contacts, and the fraction $c_s I_s/C_t$ represents the probability for an individual from the S group to have contacts with the I_s group.

We note that, if compartment sizes are held fixed, increasing σ reduces C_t, and thereby raises the instantaneous symptomatic force of infection; However, since σ also reshapes population composition and incidence over time, the overall symptomatic transmission and epidemic outcomes do not necessarily increase.

S → I_a transition. Similarly, individuals in the S class can transition to the I_a class following contact with asymptomatic individuals in classes I_a or D_a. The force of infection for the asymptomatic strain is given by

$$\lambda_a = c\beta_a \frac{c I_a + (1-\sigma)c D_a}{C_t}, \tag{2}$$

which depends on the contact rate c, the probability of transmission for the asymptomatic strain per contact, β_a, and $(c I_a + (1-\sigma)c D_a)/C_t$ represents the likelihood of having contact with people from the asymptomatic classes with the impact of SD. We assumed that asymptomatic infected individuals enter the I_a class first. Individuals in class D_a adhere to SD measures, thus contributing to the infecting susceptible individuals at a lower level than that of individuals in class I_a due to the reduced contacts $(1-\sigma)c$.

D → I_s transition. Individuals in class D practice SD by reducing their overall contact rate (contact reduction) while also avoiding interactions specifically with symptomatic individuals (contact avoidance). This reflects the fact that individuals have little incentive or ability to avoid all contacts, but are more likely to avoid visibly symptomatic persons [68,69]. As a result, the force of infection they are exposed to is different from that in the normal susceptible class. They move to class I_s at the per-capita rate

$$\lambda_s' = (1-\sigma)c\beta_s \frac{(1-\alpha)c_s I_s}{C_r}, \quad C_r = c(S + I_a + R) + (1-\sigma)c(D + D_a) + (1-\alpha)c_s I_s, \tag{3}$$

which depends on the reduced contact rate $(1-\sigma)c$, and the transmission for the symptomatic strain per contact, β_s. The fraction in Eq. (3) gives the likelihood for individuals in D class to have contact with I_s. We assumed that altered people avoid contact with symptomatic individuals with an intensity of $\alpha \in [0, 1]$. Thus, the total number of *effective* contacts from the I_s individuals is $(1-\alpha)c_s I_s$. Note that the I_s group of individuals will only alter their behavior by decreasing their contact from c to c_s. Hence, they make $c_s I_s$ contacts per unit of time. However, due to the avoidance of the D class against them, only a fraction $(1-\alpha)$ may take effect between I_s and D individuals. Similarly, we defined the total number of effective contacts from the entire population, which is given by C_r in Eq. (3). It is less than C_t in Eq. (1) due to the reduced effective contribution from I_s.

Here we briefly clarity the interpretations of σ and α. The parameter σ represents *uniform contact reduction*, setting the overall contact volume for altered individuals as $(1-\sigma)c$. In contrast, α represents *selective contact avoidance*, which modifies the mixing pattern (who interacts with whom), and it redistributes contacts away from symptomatic individuals, thereby determining the realized pool composition of contact opportunities after behavioral adjustments, C_r. Although one could alternatively embed the $(1-\alpha)$ factor into the transmission probability β_s to represent the reduced transmissibility from I_s to D, however, this would not be equivalent to the current approach, as α alters the composition of the effective contact pool, C_r.

$\boldsymbol{D \to I_a}$ transition. Individuals in class D can move to class I_a after coming into contact with individuals in classes I_a or D_a. The force of infection for D to I_a is given by

$$\lambda'_a = (1-\sigma)c\beta_a \frac{cI_a + (1-\sigma)cD_a}{C_r}. \tag{4}$$

Here, the number of contacts for the D class is $(1-\sigma)c$. Additionally, all asymptomatic infected individuals, including those who do not practice SD (I_a) and those who do practice it (D_a), contribute to the force of infection with varying weights determined by their respective number of contacts.

$\boldsymbol{I_s \to R_s}$ $\boldsymbol{(I_a, D_a \to R_a)}$ transitions. Individuals in both symptomatic and asymptomatic infection classes recover at the per capita rate γ. To focus on behavioral and evolutionary dynamics, we assume the disease-induced mortality rate to be negligible, which is reasonable when the disease-induced death rates are much lower than recovery rates.

Furthermore, our model assumes that recovery from either the symptomatic or asymptomatic strain confers lifelong immunity against both strains of the pathogen. This assumption leads our model to adopt an SIR structure.

2.2. Behavioral change

Individuals in classes S and I_a can alter their behavior by practicing SD and transition to classes D and D_a, respectively. Three main families of modeling approaches are commonly used to represent behavioral change in infectious disease dynamics: (i) *Information-index models*, where switching depends on a dynamic signal such as encounter probability with infectious individuals, reported incidence or prevalence, or media/awareness processes that accumulate and decay over time [8,10,70,71]; (ii) *Game-theoretic or payoff-based models*, where individuals adopt or imitate strategies that balance distancing costs against infection risks, often formulated using evolutionary game theory [18,19]; (iii) *Heuristic or cue-based models*, where simple perceptual cues, such as visible symptoms, trigger protective behaviors, consistent with disease-avoidance psychology [68,69].

We adopt the third approach: behavior change is assumed to be symptom-driven: individuals initiate self-distancing ($S \to D$, $I_a \to D_a$) upon encountering symptomatic individuals (I_s). This formulation captures a heuristic response to visible cues. In our setting, there is no centralized control or public communication about disease spread; behavioral responses emerge solely from local perception of visible symptoms. Individuals switch to self-distancing when a risk signal-the *information index* of d'Onofrio et al. [70]-exceeds a cue. Here, the index is the probability of encountering a symptomatic case under the current mixing pattern, a population-averaged cue that reflects symptom visibility without assuming perfect knowledge of others' activity.

The details of the model are as follows.

$\boldsymbol{S \to D}$ transition. Individuals in class S may move to class D after contact with symptomatic individuals I_s, and if they do not become infected. The force of awareness for this class is given by

$$\lambda_d = cq(1-\beta_s)\frac{c_s I_s}{C_t}, \tag{5}$$

where c is the contact rate of a susceptible individual, $(1-\beta_s)$ is the probability that infection transmission does not occur during the contact, $q \in [0,1]$ is the fraction of these individuals who change their behavior and move to class D, and $c_s I_s/C_t$ represents the probability of a symptomatic individual under the current mixing pattern.

Therefore, $c_s I_s/C_t$ serves as the adopted information index-a population-averaged measure of symptom visibility that reflects the expected likelihood of encountering a symptomatic individual. This heuristic cue represents what individuals can perceive locally (e.g., visible symptoms during interactions), rather than requiring perfect knowledge of all symptomatic individuals or their contact activity.

$\boldsymbol{I_a \to D_a}$ transition. Similarly, individuals in class I_a can have contact with people in class I_s. Although this contact does not result in infection transmission, it raises awareness for individuals in class I_a. The force of awareness for class I_a is defined as

$$\lambda'_d = cq\frac{c_s I_s}{C_t}, \tag{6}$$

where q is the fraction of people who change their behavior after being exposed to the I_s individuals.

Because awareness in our model is symptom-triggered, as more individuals move into the D or D_a classes, the denominator C_t increases and the probability of contacting a symptomatic individual decreases. This, in turn, lowers the per-capita rates λ_d and λ'_d. Therefore, the decline in those rates under widespread distancing reflects a reduced *opportunity* to encounter symptomatic infections, rather than a reduced willingness to distance.

$\boldsymbol{D \to S}$ and $\boldsymbol{D_a \to I_a}$ transitions. Being altered (remaining in classes D and D_a) can be temporary. On average, individuals stay in altered classes for $\frac{1}{\omega}$ days. Therefore, ω represents the SD waning rate.

Combining all the factors and assumptions described above, we obtain the following system:

$$\begin{aligned}
\frac{dS}{dt} &= -(\lambda_s + \lambda_a)S - \lambda_d S + \omega D,\\
\frac{dD}{dt} &= -(\lambda'_s + \lambda'_a)D + \lambda_d S - \omega D,\\
\frac{dI_a}{dt} &= \lambda_a S + \lambda'_a D - \gamma I_a - \lambda'_d I_a + \omega D_a,\\
\frac{dD_a}{dt} &= \lambda'_d I_a - \omega D_a - \gamma D_a,\\
\frac{dI_s}{dt} &= \lambda_s S + \lambda'_s D - \gamma I_s,\\
\frac{dR_a}{dt} &= \gamma(I_a + D_a),\\
\frac{dR_s}{dt} &= \gamma I_s.
\end{aligned} \tag{7}$$

Overall, in model (7), transmission proceeds through two phenotypic variants of the same pathogen: a symptomatic strain (subscript s) and an asymptomatic strain (subscript a). These strains are coupled in the force of infection terms, representing their competition for the pool of normal susceptible and altered hosts (S and D), yet they don't directly interact with each other beyond the initial infection dissemination stage.

2.3. Basic reproduction number

Using the next-generation matrix approach [72], the next-generation matrix is block-diagonal, yielding the phenotype-specific basic reproduction numbers (here we call them initial fitness) as

$$\mathcal{R}_{0a} = \frac{c\beta_a}{\gamma}, \quad \mathcal{R}_{0s} = \frac{c_s\beta_s}{\gamma}.$$

Each quantity measures a strain's ability to spread within the population: for instance, $\mathcal{R}_{0a}$, the initial fitness of the asymptomatic strain (I_a), depends on its ability to infect hosts ($c\beta_a$) and the duration of infectiousness, represented by the expected time an individual remains in the I_a compartment before recovery ($\frac{1}{\gamma}$). A similar rationale applies to $\mathcal{R}_{0s}$, which describes the fitness of the symptomatic strain (I_s), factoring in both the transmission potential ($c_s\beta_s$) and the infectious period ($\frac{1}{\gamma}$).

The overall invasion threshold for the system is then given by

$$\mathcal{R}_0 = \max\{\mathcal{R}_{0a}, \mathcal{R}_{0s}\}.$$

In the absence of joint introduction, the early dynamics follow the submodel corresponding to the introduced phenotype. When both strains are introduced simultaneously, the initial growth of infections is governed by the phenotype with the larger basic reproduction number. Accordingly, if either $\mathcal{R}_{0a} > 1$ or $\mathcal{R}_{0s} > 1$, the pathogen can successfully invade and spread in the population, consistent with classical multi-strain epidemic theory.

Global sensitivity analysis

We assess robustness to parameter uncertainty using PRCC and eFAST global sensitivity analyses. Full methodology, parameter ranges, and all additional figures/tables are provided in the Supplementary Material (Section S3).

3. Result

3.1. Parameterization

We parameterized the model based on respiratory infections, such as COVID-19. Recovery rate for COVID-19 was estimated to be around 0.1 [73], and basic reproduction number $\mathcal{R}_0$ was estimated in the range from 1.5 to 6.49, with an average of 4.2 [74,75]. The literature reports considerable variability in estimates of the relative infectiousness of symptomatic versus asymptomatic strains [76]. Some studies suggest that the asymptomatic strain has higher fitness [77,78], while others report the opposite [79,80], and some find no significant difference in dominance [81]. In this study, we focus on the impact of fitness differences between the two strains. To isolate these effects, we assume that both strains have the same initial fitness (= 4.2), in the absence of any behavioral changes. We consider three distinct scenarios to capture a range of possible outcomes:

- **B**(Baseline): Initial fitness of both strains are equal: $4.20 = \mathcal{R}_{0s} = \mathcal{R}_{0a}$. This scenario loosely reflects early-stage coexistence of similar strains, when multiple COVID-19 lineages co-circulated without clear selective dominance [81]. These patterns support the modeling assumption of roughly equal fitnesses.
- **AS**: Initial fitness of the asymptomatic strain is higher: $4.20 = \mathcal{R}_{0a} > \mathcal{R}_{0s}$. This is consistent with evidence that individuals who remain without symptoms can still transmit efficiently. For COVID-19, studies report that a large share of infections and onward transmissions originated from people who never developed symptoms [82,83]. Because such individuals are less likely to self-isolate or be detected, they sustain higher effective transmissibility at the population level.
- **SS**: Initial fitness of symptomatic strain is higher: $4.20 = \mathcal{R}_{0s} > \mathcal{R}_{0a}$. Several modeling studies estimated that symptomatic individuals are $1.75 - 2.33$ times more likely to transmit the virus than asymptomatic ones [79,80], supporting their selective advantage and a higher fitness.

We adjusted the infection spread parameters for each scenario, while adhering to the assumptions $\beta_s \geq \beta_a$ (due to the higher viral load of the symptomatic strain [84]) and $c_s \leq c$ (due to a higher likelihood of isolation for the symptomatic strain), in order to achieve fitness 4.2. All other parameters are set to replicate the recent emerging infections of COVID-19. The values are summarized in (Table 2).

We initially assumed that symptomatic and asymptomatic infections each comprised 0.5% of the population, with the remaining 99% being susceptible. All the numerical simulations were conducted in MATLAB (R2020b) using the `ode45` solver for the integration of the ODE model (7), with relative and absolute tolerances set to 10^{-10}.

3.2. Positive selection of the symptomatic strains within different contact reduction scenarios

We investigated the influence of behavioral changes via contact reduction on the transmission of symptomatic and asymptomatic viral strains. In particular, the involved behavioral change parameters include the proportion of individuals practicing SD (q), the level of contact reduction (σ), and the duration of SD ($1/\omega$). We assumed no contact avoidance ($\alpha = 0$). In this scenario, individuals engage in SD by reducing contact with everybody, triggered by the contact they made with symptomatic infected members within their social circle. This SD behavior is explored under three distinct scenarios as outlined in Section 3.1 and Table 2. The final sizes of symptomatic and asymptomatic infections were defined as the cumulative number of infected individuals for each class over the course of the outbreak, denoted by Z_s and Z_a, respectively:

$$Z_s = R_s(T), \qquad Z_a = R_a(T),$$

where T represents the end of the epidemic.

Numerically, T is determined as the earliest time when the cumulative number of removed individuals

$$R(t) = R_a(t) + R_s(t),$$

effectively stops increasing. Specifically, the integration is terminated at the first time T satisfying

$$\dot{R}(T) = \gamma\big(I_a(T) + D_a(T) + I_s(T)\big) \; < \; \varepsilon_R, \qquad \varepsilon_R = 10^{-10}.$$

For our analysis, we define and study

$$\rho_s = \frac{Z_s}{Z_s + Z_a}.$$

Given the cross-immunity assumption in our model, the definition of ρ_s provides a complementary view to the absolute final sizes Z_s and Z_a. It summarizes the competition outcome between symptomatic and asymptomatic cases by indicating the fraction of all infections ultimately attributable to the symptomatic type. In our analysis, however, ρ_s is not used in isolation but rather included as an additional summary measure to highlight the relative success of the two strains.

B(Equal initial fitness for strains): The variation in Z_s, Z_a, and ρ_s with changing σ in the range of $[0, 1]$ is illustrated in Fig. 2. The results for Z_a are straightforward: in both finite-duration and infinite-duration SD, Z_a decreases monotonically as σ increases, since individuals in this group reduce their contact more intensively under stronger distancing. Therefore, our discussion focuses on Z_s and ρ_s, whose non-monotonic trends reveal richer dynamics.

Table 2
Parameter values (with units as defined in Table 1) used in the three scenarios: **B** - equal initial fitness ($\mathcal{R}_{0a} = \mathcal{R}_{0s}$); **AS** - asymptomatic strain has higher fitness ($\mathcal{R}_{0a} > \mathcal{R}_{0s}$); **SS** - symptomatic strain has higher fitness ($\mathcal{R}_{0s} > \mathcal{R}_{0a}$). Values listed under **All Scenarios** are common across all settings. Infection parameters β_s, β_a, c, and c_s were chosen to produce $\mathcal{R}_{0a} = \mathcal{R}_{0a} = 4.2$, aligning with early COVID-19 estimates [74,75]. Parameter choices satisfy $\beta_s \geq \beta_a$ and $c_s \leq c$, reflecting plausible assumptions about transmissibility [84]. Behavioral parameters (σ, α, q, ω) lack empirical estimates and were selected to cover a broad range of plausible behaviors. Sensitivity analyses confirm that the results are robust to variation across this parameter space.

Scenario	Parameter	Value (per scenario)
B: $\mathcal{R}_{0s} = \mathcal{R}_{0a}$	β_s	0.082
	β_a	0.057
	c_s	5.10
	c	7.34
	β_s	0.085
AS: $\mathcal{R}_{0s} < \mathcal{R}_{0a}$	β_a	0.055
	c_s	4.500
	c	7.500
	β_s	0.082
SS: $\mathcal{R}_{0s} > \mathcal{R}_{0a}$	β_a	0.055
	c_s	5.100
	c	7.000
	N	10,000 (Assumed)
	γ	0.100
All Scenarios	σ	Varying in $[0, 1]$
	α	Varying in $[0, 1]$
	ω	Varying in $\{0, \frac{1}{30}, \frac{1}{90}, \frac{1}{180}, \frac{1}{360}\}$
	q	Varying in $[0, 1]$

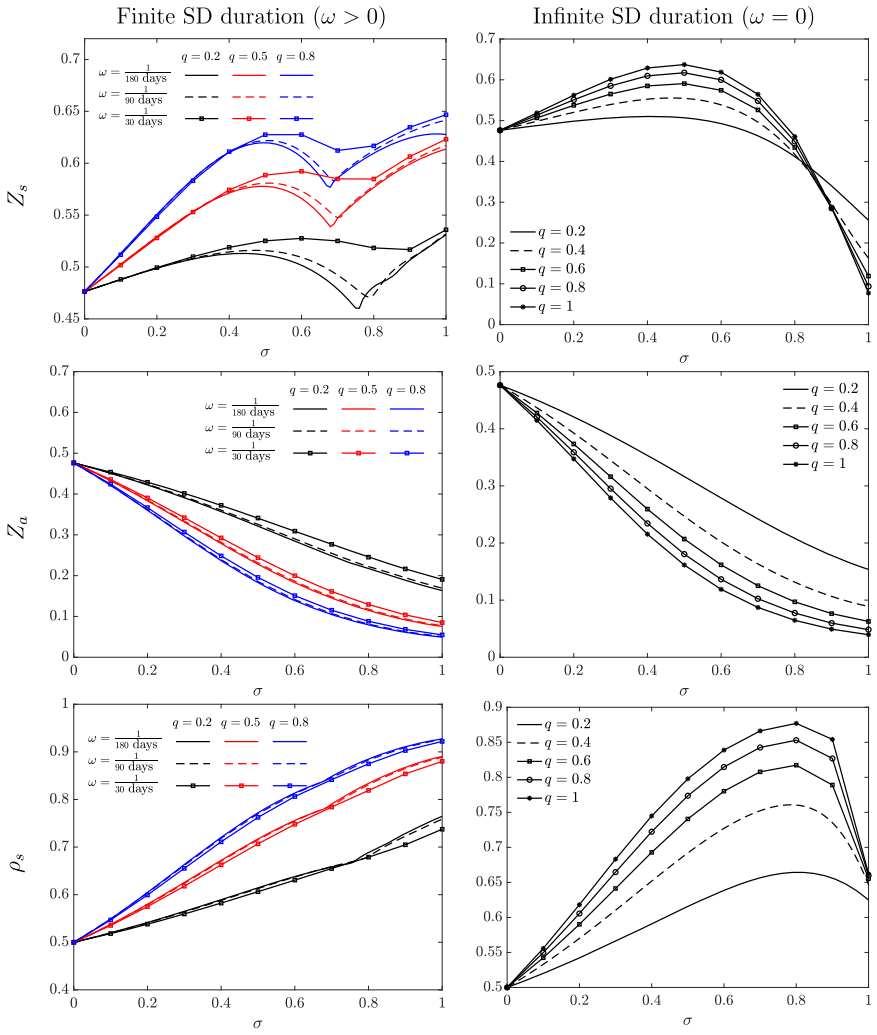

Fig. 2. Final size of symptomatic infection, Z_s, (first row), final size of asymptomatic infection, Z_a, (middle row), and relative final size of symptomatic cases, ρ_s, (last row) vs. level of SD σ for various fraction of individuals practice SD $q \in \{0.2, 0.5, 0.8\}$, and different duration of SD, $\omega \in \{0, \frac{1}{30}, \frac{1}{90}, \frac{1}{180}\}$. Both strains exhibit similar initial fitness ($\mathcal{R}_{0s} = \mathcal{R}_{0a}$).

There is a non-monotonic trend in both Z_s and ρ_s when individuals engage in SD indefinitely ($\omega = 0$): the final size of symptomatic cases increases to a maximum point as σ rises. Beyond certain high values of σ (dependent on q), however, it begins to decline. The rising portion of the plot is attributed to the fact that increasing σ not only leads individuals in class D to engage more intensely in social distancing but also prompts altered asymptomatic individuals (those in class D_a) to provide greater protection. That is, by practicing stricter social distancing, individuals in the D_a class contribute less to the spread of infection in the population. This leads to the symptomatic cases prevailing in the competition for susceptible individuals. Conversely, the declining part of the plot is a consequence of both symptomatic and asymptomatic cases being suppressed due to an extremely high (approaching isolation) level of SD. At such elevated values of σ, the effective reproduction number remains below one.

When SD duration is finite ($\omega > 0$), there exists a consistent pattern for up to moderate values of σ. However, for high levels of σ, there is a discrepancy in the results compared to those of permanent SD ($\omega = 0$). As σ increases, Z_s initially rises to a local maximum point, then starts decreasing due to infection suppression. However, it increases again by increasing σ for a very high level of SD, $\sigma > 0.75$. To understand this behavior, we plotted the time-series of symptomatic infected cases $I_s(t)$ on the left y-axis of Fig. 3 for high levels of σ and observed the second or more peaks after SD relaxation. We also approximated the effective reproduction number of the symptomatic strain, denoted by $\mathcal{R}_s(t)$. Since only individuals in classes S and $(1-\sigma)D$ are effectively susceptible to infection, and the overall contact pool is reduced due to the decreased contact rate of individuals in class D, this yields the following expression:

$$\mathcal{R}_s(t) = \mathcal{R}_{0s} \cdot \frac{S(t) + (1-\sigma)D(t)}{N - \sigma D(t)}. \tag{8}$$

The time series of $\mathcal{R}_s(t)$ is plotted on the right y-axis of Fig. 3. The results show a correlation between $\mathcal{R}_s(t)$ and the rebound behavior of symptomatic cases: When σ is not big enough (the first column of Fig. 3), $\mathcal{R}_s(t)$ always stays below one, and $I_s(t)$ dies out after passing the first peak. However, when σ is very big (the second and third columns of Fig. 3), $\mathcal{R}_s(t)$ goes beyond one, and with a short time lag, another peak of symptomatic infection occurs. One striking result is that the number of rebounds (the peaks after the first peak) is equal to the number of times $\mathcal{R}_s(t)$ goes beyond one. The reason is SD relaxation, where individuals practice SD for a limited time, and after passing the limited time, they return to class S, thus increasing S while decreasing D. Because the coefficient $(1-\sigma)$ is small, the term $(1-\sigma)D$ is also small, and σD is negligible compared to N. Consequently, the D class does not significantly affect $\mathcal{R}_s(t)$. This increment in the S class provides a more susceptible pool for symptomatic infection spread, as the asymptomatic strain died out during the first intense SD times.

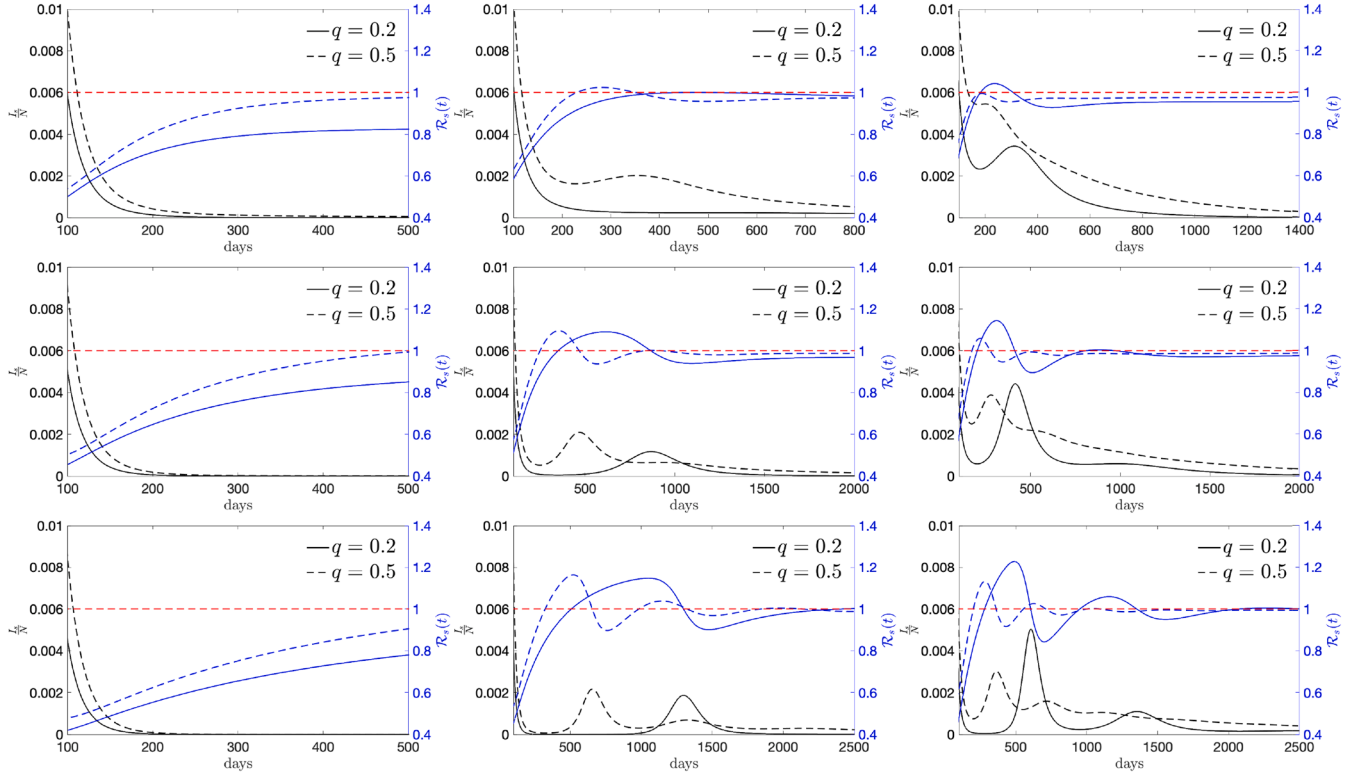

Fig. 3. The time-series illustrating symptomatic cases and the symptomatic reproduction number for different combinations of the parameters σ and ω, as well as other parameters defined in scenario **B**. The parameter ω is set at $\omega = \frac{1}{90}$, $\omega = \frac{1}{180}$, and $\omega = \frac{1}{360}$ in the first, second, and third row, respectively. The parameter σ varies across the columns with values $\sigma = 0.7$, $\sigma = 0.8$, and $\sigma = 0.9$ in the first, second, and third columns, respectively. The time axis begins after the first peak ($t = 100$). The black curves, depicting the proportion of symptomatic cases $\frac{I_s(t)}{N}$, are aligned with the left y-axis. Meanwhile, the blue curves, representing the symptomatic reproduction number $\mathcal{R}_s(t)$, are aligned with the right y-axis. The dashed red line indicates the point where $\mathcal{R}_s(t) = 1$. We note that the extended time horizon (up to 2500 days) is shown only to capture all rebounds and eventual extinction under fixed model parameters, and is not intended to imply persistence of epidemics for seven years in practice.

We also point out that because the model has an SIR structure without waning or demographic turnover, the susceptible population is not replenished. The behavioral feedback between S and D is bounded and delay-free, depending on the current encounter probability with symptomatic individuals and relaxing at a constant rate. As a result, the feedback introduces dissipation rather than phase lag, leading to damped rebounds rather than sustained oscillations.

The apparent kinks in $Z_s(\sigma)$ for $\omega > 0$ therefore occur when increasing σ moves the system across thresholds where the post-relaxation effective reproduction number $\mathcal{R}_s(t)$ crosses one. At these threshold values, the epidemic trajectory changes qualitatively—for instance, from a single wave to multiple waves—leading to visible kinks in the final-size curve. The curve itself remains continuous, but its slope changes abruptly, which gives the appearance of non-smoothness.

AS (Initial fitness of asymptomatic strain is bigger than that of symptomatic one): The variation in Z_s, Z_a, and ρ_s with changing σ in the range of $[0, 1]$ is illustrated in Fig. 4. The results for Z_a, similar to the previous scenario, are straightforward: higher levels of SD lead to a more pronounced decrease in the asymptomatic final size. The results for Z_s and ρ_s, however, are worth further explanation.

When the duration of social distancing (SD) extends to 90 days or more, the non-monotonic behavior of Z_s concerning σ becomes evident. This is illustrated in the left panel of Fig. 4. The rationale behind the non-monotonic behavior of Z_s aligns with the previous scenario: The upward trend is attributed to the fact that an increase in σ leads to enhanced protection from altered asymptomatic individuals (those in class D_a), creating conditions for symptomatic cases to target more susceptible cases. Conversely, the downward trend is a result of virus suppression through a high level of SD. However, due to the fact that $\mathcal{R}_{0a} > \mathcal{R}_{0s}$, there are more asymptomatic infected cases than symptomatic ones. This, in turn, causes the change in non-monotonic behavior of Z_s in scenario **AS** to exhibit a slower pace than in scenario **B**. In other words, the variation in Z_s in scenario **AS** is less pronounced than that in scenario **B**. Also, dominance of initial fitness for asymptomatic strain keeps the symptomatic burden low, so the threshold-crossing mechanism that generates the observed kink at scenario **B** is effectively masked here.

For a shorter SD duration ($\omega = \frac{1}{30}$), the value of Z_s increases and levels off to a constant value as σ increases. The upward trend is consistent with the previous explanation. However, the reason it does not decrease for high values of σ is that the intense level of SD is compensated by its short duration. In other words, individuals return to their normal behavior shortly after a brief period, before the number of infected cases becomes sparse. This prevents the effective suppression of infection through sustained SD practices.

In contrast to scenario **B**, the proportion of symptomatic cases (ρ_s) consistently rises as σ increases, see right panel of Fig. 4. This trend is attributed to the combined effects of a) the growing portion of Z_s and b) a more substantial decline in asymptomatic cases during virus suppression (the decreasing segment of Z_s) owing to its higher initial fitness.

SS (Initial fitness of symptomatic strain is bigger than that of asymptomatic one): The last scenario studies the case that the initial fitness of the symptomatic strain is higher than that of the asymptomatic one ($\mathcal{R}_{0s} > \mathcal{R}_{0a}$), see Fig. 5. In this scenario, we observe a consistent decrease in Z_s and Z_a. While a decrease in Z_a is due to more intense SD, the reason behind the decrease in Z_s lies in the smaller initial fitness of asymptomatic cases, leading to a majority of the infected population exhibiting symptoms. Consequently, there are fewer asymptomatic cases

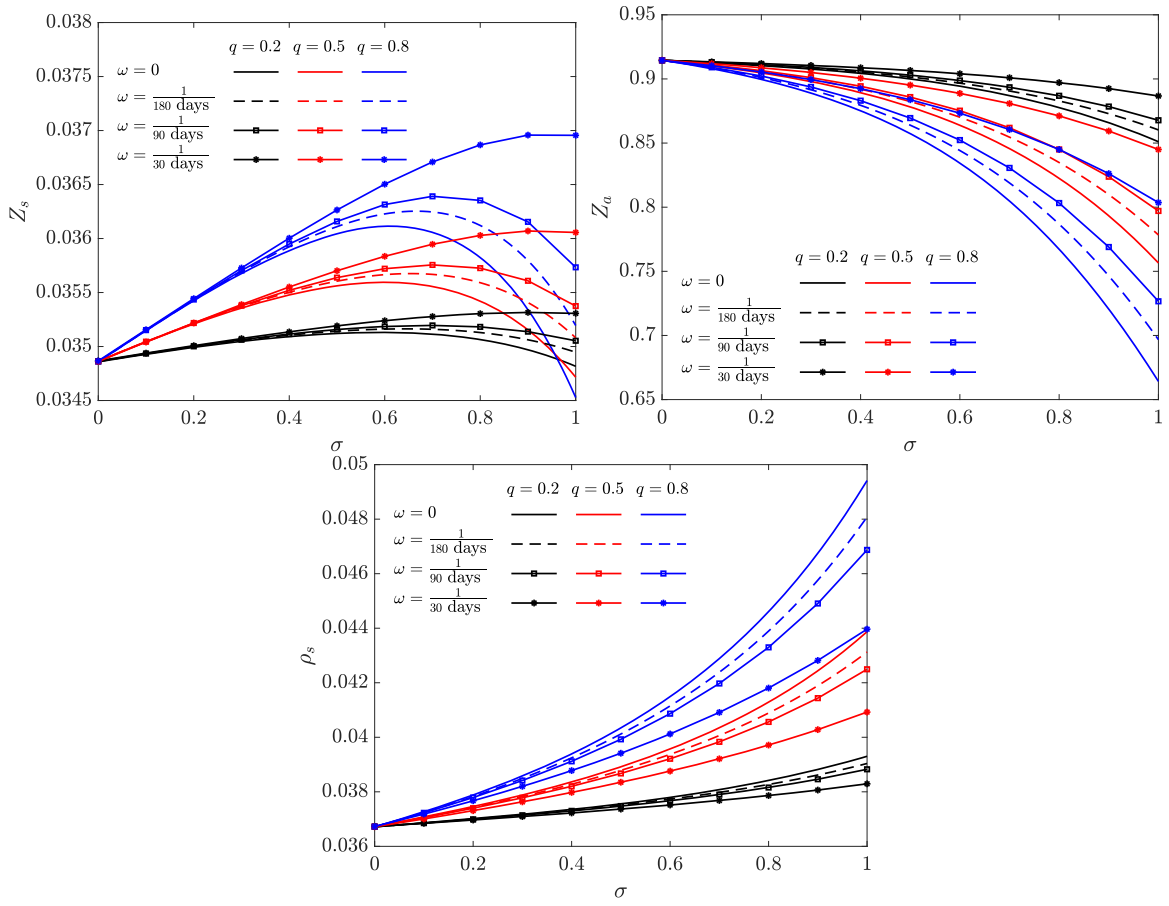

Fig. 4. Final size of symptomatic infection, Z_s, (top left panel), final size of asymptomatic infection, Z_a, (top right panel), and relative final size of symptomatic cases, ρ_s, (bottom panel) vs. level of SD σ for various fraction of individuals practice SD $q \in \{0.2, 0.5, 0.8\}$, and different duration of SD, $\omega \in \{0, \frac{1}{30}, \frac{1}{90}, \frac{1}{180}\}$. Asymptomatic strain exhibits higher initial fitness than the symptomatic one ($\mathcal{R}_{0s} < \mathcal{R}_{0a}$).

competing with symptomatic ones. As a result, the system behaves almost similarly to a single-strain model, where the implementation of any type of SD causes a reduction in the final size. It is important to note that despite being smaller than $\mathcal{R}_{0s}$, $\mathcal{R}_{0a}$ is still greater than one. Thus, an outbreak of the asymptomatic strain occurs, but it is negligible compared to the symptomatic one.

3.3. Contact avoidance selects for asymptomatic strain

To explore how (partially) avoiding symptomatic cases, controlled by the parameter α, affects the outcomes discussed in the previous subsection, we conducted simulations using the Model Eq. (7) across various levels of SD, σ and α, within three distinct scenarios **B**, **AS**, and **SS**.

B (Equal initial fitness for strains): Fig. 6 illustrates the final sizes of strains for the case where $q = 0.5$, $\omega = 0$ (the first row) and $\omega = \frac{1}{30}$ (the second row), with the transmission parameter selected under scenario **B**.

When individuals practice SD indefinitely ($\omega = 0$), the final size of symptomatic cases Z_s shows a clear non-monotonic dependence on σ at low avoidance levels, reproducing the rebound pattern of Fig. 2. As avoidance increases, the effect of σ weakens and Z_s decreases overall, so the non-monotonicity is gradually lost, see top left panel of Fig. 6. The one–dimensional summary of this two–dimensional pattern in the heatmap clarifies how the apparent color gradients translate into the shape of $Z_s(\sigma)$ at fixed α. This inset extracts two horizontal slices of the heatmap-at $\alpha = 0.1$ (solid) and $\alpha = 0.6$ (dashed)-and plots the corresponding curves $Z_s(\sigma)$ on common axes. The horizontal dashed guide in the panel indicates the slice at $\alpha = 0.6$. This makes explicit that, for weak avoidance, $Z_s(\sigma)$ initially increases and then decreases (a rebound), whereas under stronger avoidance the non-monotonicity is diminished. On the other hand, the final size of asymptomatic cases Z_a shows an intuitive result; it is maximized at the top left corner; when individuals strictly avoid symptomatic cases but maintain contact with others, i.e., when σ is very small and α is high. The arrow in the top-left panel of Fig. 6 indicates the direction that leads to larger values of Z_a.

For temporary SD ($\omega = \frac{1}{30}$), the second row in Fig. 6 show opposite strategies for maximizing the two strains. Maximizing Z_s (while minimizing Z_a) occurs when σ is high and α is low, i.e., when individuals reduce their overall contacts strongly, but do not specifically avoid symptomatic cases. In this regime, symptomatic infections remain socially active and capture more of the susceptible pool. Conversely, maximizing Z_a (while minimizing Z_s) occurs when σ is low and α is high, i.e., when individuals maintain most of their contacts but strongly avoid visibly symptomatic cases. Here, avoidance of symptomatic individuals leaves a larger pool of susceptibles available for the asymptomatic strain. Because the total final size does not decrease much for such short distancing, these patterns highlight the competition between the two strains, with σ and α representing two distinct behavioral pathways that determine which strain dominates. Notably, the kink observed in the longer SD case (Fig. 2) is not pronounced here, as the shorter distancing period limits the rebound dynamics.

The result for overall final size, $Z_s + Z_a$ in both cases of $\omega = 0$ or $\frac{1}{30}$ are shown in supplementary material, first row of Fig. S1.

AS (Initial fitness of asymptomatic strain is bigger than that of symptomatic one): Fig. 7 depicts the same experiment as shown in Fig. 6, for the case that the transmission parameters are chosen under scenario **AS**, higher initial fitness for the asymptomatic strain. First, an examination of the color bar values reveals that the majority of the total

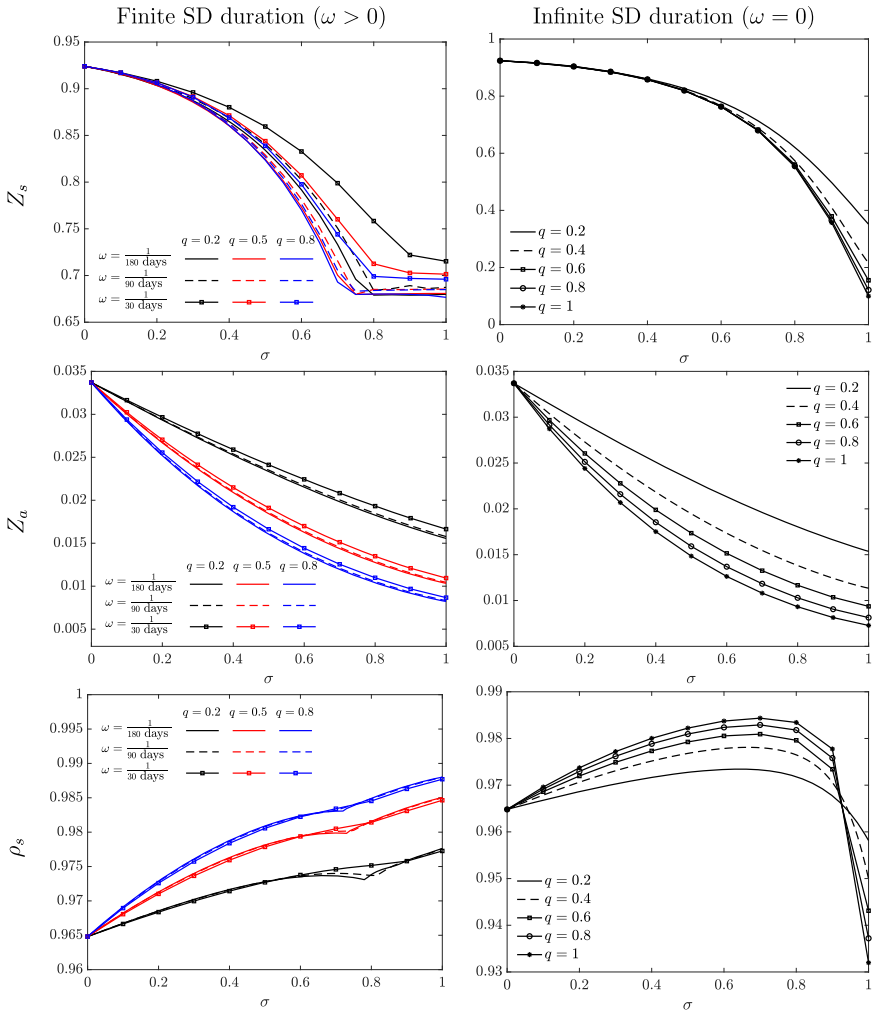

Fig. 5. Final size of symptomatic infection, Z_s, (first row), final size of asymptomatic infection, Z_a, (middle row), and relative final size of symptomatic cases, ρ_s, (last row) vs. fraction of individuals practice SD, q, vs. intensity of SD, σ, for different duration of SD, $\omega \in \{0, \frac{1}{30}, \frac{1}{90}, \frac{1}{180}\}$, when $\mathcal{R}_{0s} > \mathcal{R}_{0a}$.

final size is attributed to asymptomatic cases due to their higher initial fitness. Although the quantity of Z_s is negligible compared to that of Z_a, it can still be controlled by α and σ.

Similar to scenario **B**, with indefinite SD ($\omega = 0$) in the first row of Fig. 7, the final size of symptomatic cases Z_s depends non-monotonically on σ when avoidance is weak, showing the non-monotonicity seen in Fig. 4. As α increases, the influence of σ on Z_s increases, while the non-monotonicity trend disappears. The inset in the top left panel of Fig. 7 extracts two horizontal slices of the heatmap-at $\alpha = 0.05$ (solid) and $\alpha = 0.5$ (dashed)-and plots the corresponding one–dimensional curves $Z_s(\sigma)$ on common axes. This makes explicit that for weak avoidance ($\alpha = 0.05$), $Z_s(\sigma)$ initially increases and then decreases (a rebound), whereas for stronger avoidance ($\alpha = 0.5$) it is monotone increasing. Mitigating symptomatic cases with varying intensity (by altering α) does not significantly affect Z_a since there are not too many symptomatic cases compared to asymptomatic ones. But, decreasing σ results in a larger proportion of asymptomatic cases.

When the duration of SD is short ($\omega = \frac{1}{30}$ in the second row of Fig. 7), the non-monotonicity in $Z_s(\sigma)$ disappears entirely. As in scenario **B**, increasing σ and decreasing α produce more symptomatic cases, though the effect is weaker due to the higher fitness of asymptomatic cases. The behavior of Z_a remains the same as under indefinite SD: varying α has little influence because symptomatic cases are few, while reducing σ increases the proportion of asymptomatic cases.

The result for overall final size, $Z_s + Z_a$ in both cases of $\omega = 0$ or $\frac{1}{30}$ are shown in supplementary material, second row of Fig. S1.

SS (Initial fitness of symptomatic strain is bigger than that of asymptomatic one): The final experiment pertains to a scenario denoted as **SS**, where the initial fitness of the symptomatic strain surpasses that of the asymptomatic one. The outcomes of this experiment are illustrated in Fig. 8.

The first row of Fig. 8 corresponds to $\omega = 0$, i.e., permanent SD. Z_s is maximized at low SD (small α and σ) and declines as SD (in any type) intensifies. In contrast, Z_a remains small across most SD levels due to its lower fitness but rises when σ is low and α is very high (top-right corner), since individuals avoid symptomatic cases while still allowing spread of the asymptomatic strain. The arrows in Fig. 8 indicate the directions in (σ, α) space that maximize Z_s (left panel) and Z_a (right panel).

The second row of Fig. 8 pertains to temporary SD with $\omega = \frac{1}{30}$. The behavior of Z_a remains consistent with the previous case of $\omega = 0$, because of the dominance of infection by the symptomatic strain. For Z_s, the dynamics are more nuanced. First, for any value of σ, increasing α reduces Z_s. This reduction weakens as σ grows, and for $\sigma \gtrsim 0.8$ the marginal influence of α becomes negligible. Second, the effect of σ on Z_s depends on α: when α is small, σ reduces Z_s (i.e., $Z_s(\sigma)$ decreases), consistent with Fig. 5. In contrast, at higher α, the trend reverses-$Z_s(\sigma)$ increases with σ. This is because strong avoidance of symptomatic cases by

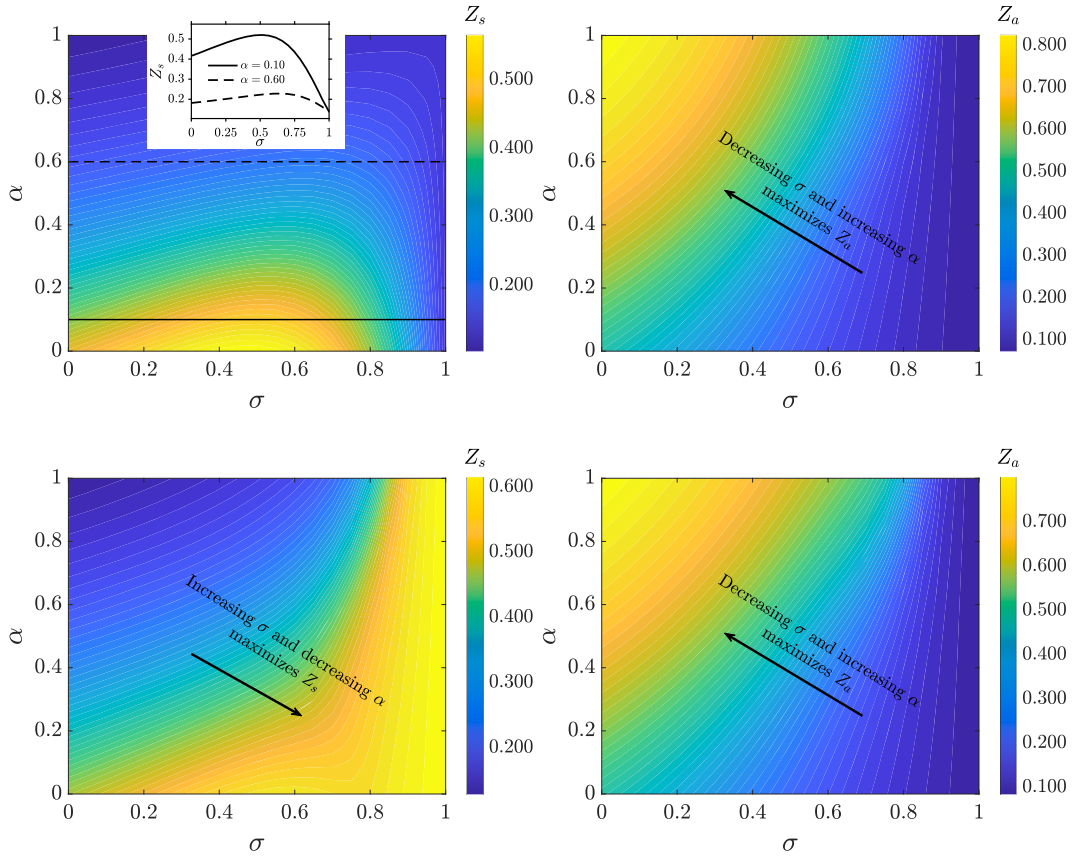

Fig. 6. Final sizes vs. SD levels α and σ, Left: Z_s (symptomatic); Right: Z_a (asymptomatic). This is done for various levels of SD strategies (σ and α). The parameter values are set at $q = 0.5$, $\omega = 0$ (first row), and $\omega = \frac{1}{30}$ (second row), with transmission parameters selected based on scenario **B** in Table 2.

α leaves σ acting mainly on asymptomatic transmission, indirectly favoring symptomatic spread and thus opposing α. The inset in the left panel extracts two horizontal slices of the heatmap-at $\alpha = 0.05$ (solid) and $\alpha = 0.8$ (dashed)-and plots the corresponding one–dimensional curves $Z_s(\sigma)$ on common axes. The solid curve shows the decreasing relationship at weak avoidance ($\alpha = 0.05$), whereas the dashed curve shows the reversed, increasing trend under strong avoidance ($\alpha = 0.8$). The proximity of the two curves for large σ also visualizes how the impact of α vanishes at high contact reduction.

The result for overall final size, $Z_s + Z_a$ in both cases of $\omega = 0$ or $\frac{1}{30}$ are shown in supplementary material, third row of Fig. S1.

3.4. Global sensitivity analysis

The sensitivity analysis (Section S3 in Supplementary material) shows transmission parameters dominate, with notable effects of the behavioral parameters σ and α. Increasing σ (uniform contact reduction) has little effect on the symptomatic final size but reduces the asymptomatic final size, lowering the total. Increasing α (targeted avoidance of symptomatics) decreases the symptomatic final size while increasing the asymptomatic one; the total still declines, but less than under higher σ. Thus, broad contact reduction is more effective for minimizing overall contagion.

Although final sizes show limited dependence on behavioral parameters, time-resolved sensitivity reveals periods when the symptomatic share ρ_s and effective reproduction number $R_s(t)$ are highly responsive to behavior. Higher transmission probability (or lower SD) produces an early surge in sensitivity that later declines (Supplementary Material, Fig. S4, top), consistent with [85]. By contrast, the SD level begins with negligible sensitivity and then stabilizes at a higher, sustained influence (Fig. S4, bottom).

4. Discussion

4.1. Motivation and innovation in this study

As documented by various studies [12,27,86–89], human behavior can undergo changes in response to diseases observed in their surroundings. These behavioral shifts play a crucial role in the spread of epidemics [8,90–92]. It has been observed that human behavioral traits related to disease avoidance undergo selection in the presence of infectious diseases [51]. In this context, we explored how behavioral responses to symptoms can shift the relative fitness of symptomatic versus asymptomatic strains of the same pathogen.

We employed an SIR-structured ODE model that incorporates two distinct dynamics: infection dynamics and behavioral changes. This model was utilized to investigate the spread of two co-circulating virus strains, namely symptomatic and asymptomatic. We implemented a form of spontaneous social distancing, as described in Azizi et al. [89]. In this approach, susceptible and asymptomatic infected individuals make decisions to protect themselves based on the infection status of their contacts. Specifically, they reduce a certain fraction of their contacts if they come across a symptomatically infected individual among them.

4.2. Impact of behavioral change on strains' final size

The impact of behavioral change parameters on the final size of each strain was investigated through simulations in three different scenarios: a) equal initial fitness for both strains, b) higher initial fitness for the asymptomatic one, and c) higher initial fitness for the symptomatic one. For the first two cases, where the initial fitness of the symptomatic strain is smaller or equal to that of the asymptomatic one, the symptomatic final size Z_s and its proportion ρ_s exhibit a non-monotonic behavior

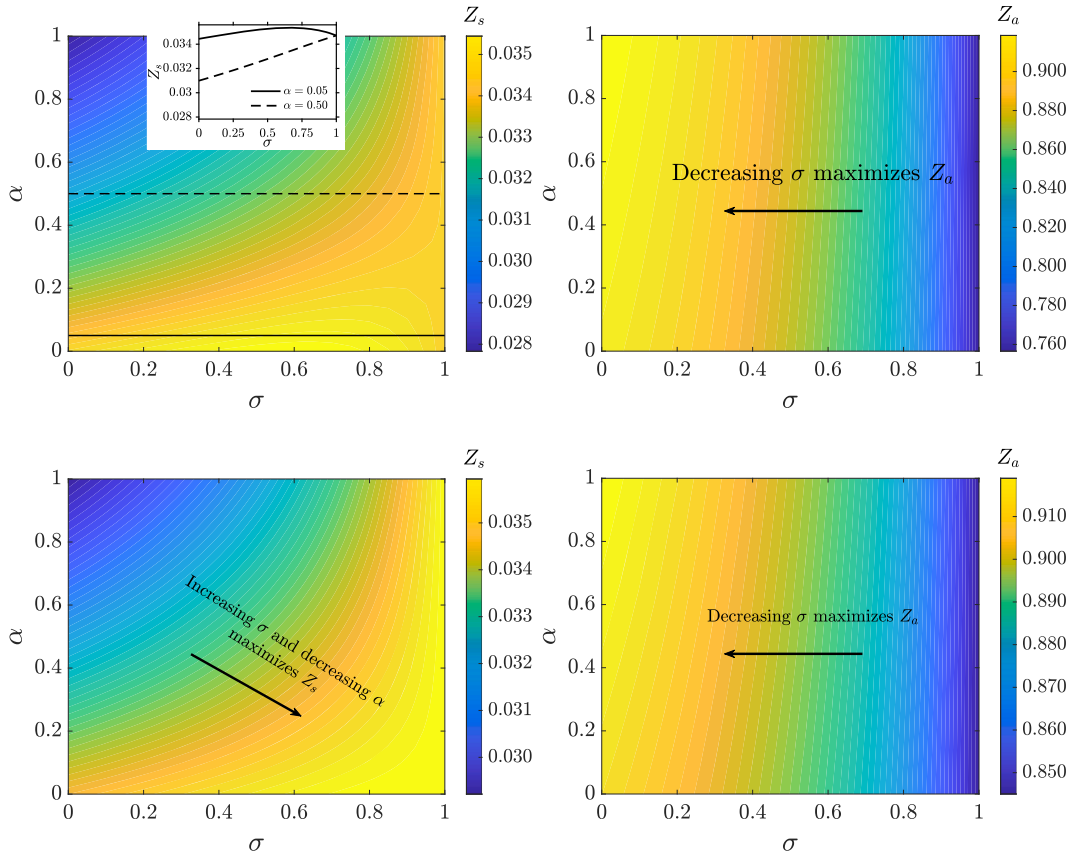

Fig. 7. Final sizes vs. SD levels α and σ, Left: Z_s (symptomatic); Right: Z_a (asymptomatic). This is done for various levels of SD strategies (σ and α). The parameter values are set at $q = 0.5$, $\omega = 0$ (first row), and $\omega = \frac{1}{30}$ (second row), with transmission parameters selected based on the scenario **AS** in Table 2.

with respect to SD level denoted by σ, see Figs. 2 and 4. In these cases, as altered individuals reduce their contact more intensely, the share of symptomatic cases increases unless the reduction in contact is substantial enough to suppress both strains. Notably, when altered individuals practice SD temporarily but intensely, a shift in symptomatic cases occurs; The symptomatic strain experiences a second or subsequent peaks, while the asymptomatic strain almost diminishes with only one peak. However, when the initial fitness of the symptomatic strain is higher, the model behaves like a single-strain one, where an increase in SD level leads to a decrease in the final size of the infection. As an intuitive consequence, all non-monotonic (or monotonic) trends of symptomatic final size as a function of σ in three different scenarios are mitigated toward reducing symptomatic cases when altered individuals partially avoid contacting symptomatic cases ($\alpha > 0$).

4.3. Limitations of the study and future work

The proposed model, akin to other studies in mathematical modeling, benefits from the ability to explore biological issues in a virtual environment, striving to replicate real-world scenarios. But, the results should not be interpreted as an accurate quantitative prediction of real-world outcomes. Instead, they are framed as an explorative scenario analysis; that is, the purpose of the simulation is to understand the potential dynamics and effects of different parameters rather than provide precise predictions.

Modeling human behavior is inherently challenging, and our framework necessarily relies on simplifying assumptions. One limitation of our study is that we focus on a single behavioral trigger-direct encounters with symptomatic individuals-implemented via a heuristic symptom–cued rule. We do not explicitly model awareness–contagion or incidence-based information, which are central in other behavior–disease frameworks [71]. Our results should therefore be viewed as a baseline characterization of selection under symptom visibility alone. Extending the model to couple symptom-based cues with richer information processes (awareness spread, risk perception from reported incidence, and institutional messaging) is an important direction for future work. We also assume that individuals cut off contact once they detect a symptomatically infected person in their social circle, without distinguishing between different types of contact. We omit demographic and socioeconomic factors that could influence people's ability to adopt protective behaviors, as well as interventions such as vaccination or government-mandated social distancing. To address these limitations, future work will expand the model by integrating a coupled infection–information framework, where social distancing and vaccination are triggered by the spread of (mis)information. It also will incorporate reporting delays/noise and heterogeneity in awareness, and allow time-varying SD to capture a more realistic behavioral change model. Finally, our current model fixes symptom propensity at the strain level: infections remain either symptomatic or asymptomatic throughout a transmission chain, and no mutation between strains is allowed. While this assumption captures stable strain-level differences, future extensions could incorporate host-modulated switching or evolutionary transitions between strains to test the robustness of our conclusions.

Despite these limitations, our analysis robustly demonstrates that human behavior in response to an infection outbreak can influence the various manifestations of a virus [89]. Specifically, exercising caution when coming into contact with symptomatic cases can contribute to the emergence ofa virus that induces more symptomatic disease. Although we have not specifically modeled a particular infection, our modeling approach is designed to depict generic respiratory infections transmitted through physical contact. As a result, it holds relevance for the future emerging or reemerging infections.

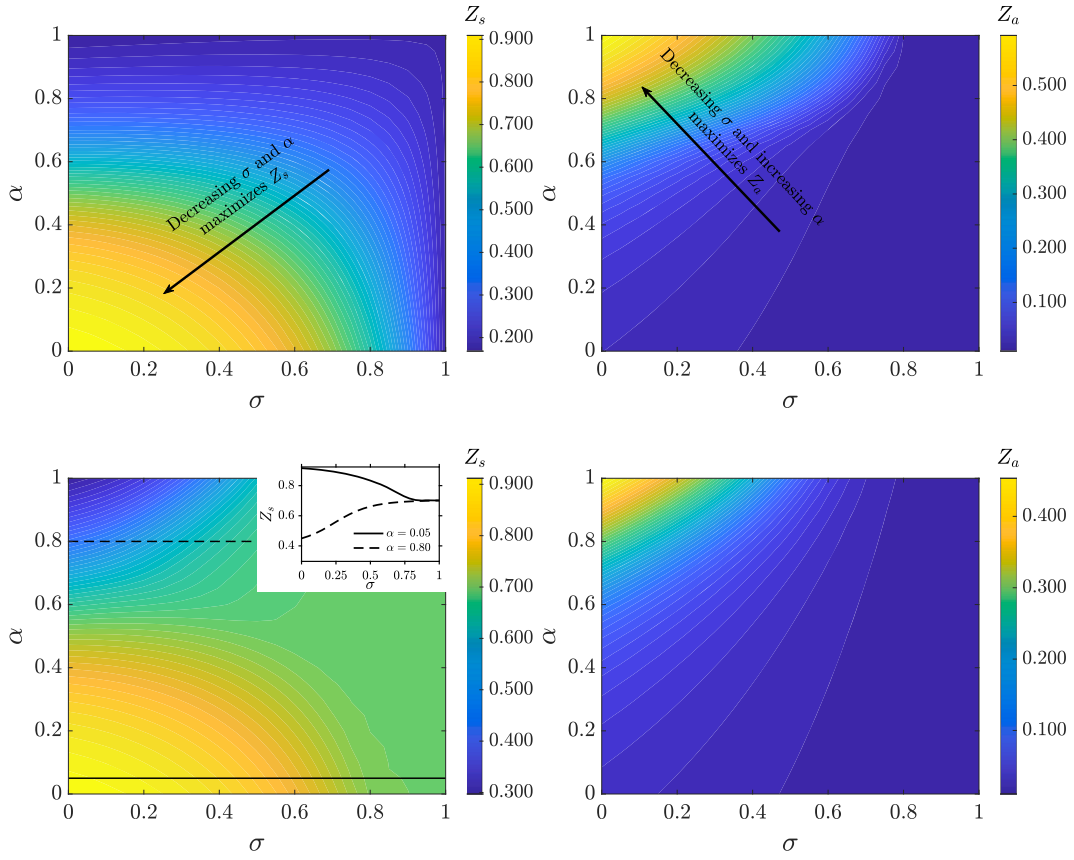

Fig. 8. Final sizes vs. SD levels α and σ, Left: Z_s (symptomatic); Right: Z_a (asymptomatic). This is done for various levels of SD strategies (σ and α). The parameter values are set at $q = 0.5$, $\omega = 0$ (first row), and $\omega = \frac{1}{30}$ (second row), with transmission parameters selected based on the scenario **SS** in Table 2.

CRediT authorship contribution statement

Asma Azizi: Writing – review & editing, Writing – original draft, Visualization, Methodology, Conceptualization; **Zhuolin Qu:** Writing – review & editing, Methodology; **Caner Kazanci:** Writing – review & editing, Methodology.

Contributors

All authors contributed to the design of the mathematical model. AA conducted the numerical simulations, handled visualization, interpreted the results, and wrote the initial draft of the paper. ZQ and CK reviewed the model design and interpretation. CK also contributed to the simulations and optimized the code. ZQ provided input in writing and reviewed the draft. All authors approved the final manuscript.

Funding

This research did not receive any specific grant from funding agencies.

Data availability

No data was used for the research described in the article.

Declaration of interests

The authors declare that they have no known competing financial interests or personal relationships that could have appeared to influence the work reported in this paper.

Supplementary material

Supplementary material associated with this article can be found, in the online version, at 10.1016/j.mbs.2025.109601

References

[1] G.J. Rubin, R. Amlôt, L. Page, S. Wessely, Public perceptions, anxiety, and behaviour change in relation to the swine flu outbreak: cross sectional telephone survey, BMJ 339 (2009).
[2] V. Freimuth, H.W. Linnan, P. Potter, Communicating the threat of emerging infections to the public, Emerg. Infect. Dis. 6 (4) (2000) 337.
[3] T. Yamanis, E. Nolan, S. Shepler, Fears and misperceptions of the Ebola response system during the 2014–2015 outbreak in Sierra Leone, PLoS Negl. Trop. Dis. 10 (10) (2016) e0005077.
[4] P. Sheeran, P.R. Harris, T. Epton, Does heightening risk appraisals change people's intentions and behavior? A meta-analysis of experimental studies, Psychol. Bull. 140 (2) (2014) 511.
[5] R.A. Ferrer, W.M.P. Klein, Risk perceptions and health behavior, Curr. Opin. Psychol. 5 (2015) 85–89.
[6] P. Phang, B. Wiwatanapataphee, Y.H. Wu, Social and economic influences on human behavioural response in an emerging epidemic, in: Journal of Physics: Conference Series, 893, IOP Publishing, 2017, p. 012017.
[7] P. Manfredi, A. d'Onofrio (Eds.), Modeling the Interplay Between Human Behavior and the Spread of Infectious Diseases, Springer, New York, 2013.
[8] S. Funk, M. Salathé, V.A.A. Jansen, Modelling the influence of human behaviour on the spread of infectious diseases: a review, J, Roy, Soc. Interface 7 (50) (2010) 1247–1256.
[9] Z. Wang, C.T. Bauch, S. Bhattacharyya, A. d'Onofrio, P. Manfredi, M. Perc, N. Perra, M. Salathé, D. Zhao, Statistical physics of vaccination, Phys. Rep. 664 (2016) 1–113. https://doi.org/10.1016/j.physrep.2016.10.006
[10] F. Verelst, L. Willem, P. Beutels, Behavioural change models for infectious disease transmission: a systematic review, J. Roy. Soc. Interface 13 (125) (2016) 20160820. https://doi.org/10.1098/rsif.2016.0820
[11] J. Bedson, L.A. Skrip, D. Pedi, S. Abramowitz, S. Carter, M.F. Jalloh, S. Funk, N. Gobat, T. Giles-Vernick, C. Déglise, et al., Community engagement during outbreak response: capabilities and challenges revealed during the 2014–2016 Ebola

epidemic, Nat. Hum. Behav. 5 (12) (2021) 1634–1647. https://doi.org/10.1038/s41562-021-01113-x
[12] A. Azizi, C. Montalvo, B. Espinoza, Y. Kang, C. Castillo-Chavez, Epidemics on networks: reducing disease transmission using health emergency declarations and peer communication, Infect. Dis. Modell. 5 (2020) 12–22.
[13] J.M. Epstein, J. Parker, D. Cummings, R.A. Hammond, Coupled contagion dynamics of fear and disease: mathematical and computational explorations, PLoS ONE 3 (12) (2008) e3955.
[14] F.D. Sahneh, F.N. Chowdhury, C.M. Scoglio, On the existence of a threshold for preventive behavioral responses to suppress epidemic spreading, Sci. Rep. 2 (2012) 632.
[15] N. Perra, D. Balcan, B. Gonçalves, A. Vespignani, Towards a characterization of behavior-disease models, PLoS ONE 6 (8) (2011) e23084.
[16] I.Z. Kiss, J. Cassell, M. Recker, P.L. Simon, The impact of information transmission on epidemic outbreaks, Math. Biosci. 225 (1) (2010) 1–10.
[17] A.K. Misra, A. Sharma, J.B. Shukla, Modeling and analysis of effects of awareness programs by media on the spread of infectious diseases, Math. Comput. Model. 53 (5–6) (2011) 1221–1228.
[18] P. Poletti, M. Ajelli, S. Merler, The effect of risk perception on the 2009 H1N1 pandemic influenza dynamics, PLoS ONE 6 (2) (2011) e16460.
[19] P. Poletti, M. Ajelli, S. Merler, Risk perception and effectiveness of uncoordinated behavioral responses in an emerging epidemic, Math. Biosci. 238 (2) (2012) 80–89.
[20] P. Poletti, B. Caprile, M. Ajelli, A. Pugliese, S. Merler, Spontaneous behavioural changes in response to epidemics, J. Theor. Biol. 260 (1) (2009) 31–40.
[21] J.M. Hyman, J. Li, Infection-age structured epidemic models with behavior change or treatment, J. Biol. Dyn. 1 (1) (2007) 109–131.
[22] S.M. Tracht, S.Y. Del Valle, J.M. Hyman, Mathematical modeling of the effectiveness of facemasks in reducing the spread of novel influenza a (H1N1), PLoS ONE 5 (2) (2010) e9018.
[23] Q. Wu, X. Fu, M. Small, X.-J. Xu, The impact of awareness on epidemic spreading in networks, Chaos: Interdiscipl. J, Nonlinear Sci. 22 (1) (2012) 013101.
[24] S. Funk, E. Gilad, C. Watkins, V.A.A. Jansen, The spread of awareness and its impact on epidemic outbreaks, Proceed. Natl. Acad. Sci. 106 (16) (2009) 6872–6877.
[25] C. Granell, S. Gómez, A. Arenas, Dynamical interplay between awareness and epidemic spreading in multiplex networks, Phys. Rev. Lett. 111 (12) (2013) 128701.
[26] S. Meloni, N. Perra, A. Arenas, S. Gómez, Y. Moreno, A. Vespignani, Modeling human mobility responses to the large-scale spreading of infectious diseases, Sci. Rep. 1 (2011) 62.
[27] N.L. Komarova, A. Azizi, D. Wodarz, Network models and the interpretation of prolonged infection plateaus in the COVID19 pandemic, Epidemics 35 (2021) 100463.
[28] C. Fraser, S. Riley, R.M. Anderson, N.M. Ferguson, Factors that make an infectious disease outbreak controllable, Proceed. Natl. Acad. Sci. 101 (16) (2004) 6146–6151.
[29] A. Azizi, C. Kazanci, S. Lee, Adaptive social distancing strategies for controlling infection inequality in emerging infectious diseases, Lett. Biomath. 10 (1) (2023) 149.
[30] C.T. Bauch, Imitation dynamics predict vaccination behaviour, Proceed. Roy. Soc. B: Biolog. Sci. 272 (1573) (2005) 1669–1676. https://doi.org/10.1098/rspb.2005.3153
[31] A. d'Onofrio, P. Manfredi, E. Salinelli, Vaccinating behaviour, information, and the dynamics of SIR vaccine preventable diseases, J. Theor. Biol. 273 (1) (2011) 63–71. https://doi.org/10.1016/j.jtbi.2010.12.035
[32] A. d'Onofrio, P. Manfredi, P. Poletti, The impact of vaccine side effects on the dynamics of vaccination coverage and social contact: a behavioural modelling approach, PLoS ONE 7 (12) (2012) e50701. https://doi.org/10.1371/journal.pone.0050701
[33] C.R. Parrish, E.C. Holmes, D.M. Morens, E.-C. Park, D.S. Burke, C.H. Calisher, C.A. Laughlin, L.J. Saif, P. Daszak, Cross-species virus transmission and the emergence of new epidemic diseases, Microbiol. Molecul. Biol, Rev. 72 (3) (2008) 457–470.
[34] K.A. Twohig, T. Nyberg, A. Zaidi, S. Thelwall, M.A. Sinnathamby, S. Aliabadi, S.R. Seaman, R.J. Harris, R. Hope, J. Lopez-Bernal, et al., Hospital admission and emergency care attendance risk for SARS-CoV-2 delta (B. 1.617. 2) compared with alpha (B. 1.1. 7) variants of concern: a cohort study, Lancet Infect. Dis. 22 (1) (2022) 35–42.
[35] K.A. Twohig, T. Nyberg, A. Zaidi, S. Thelwall, et al., Hospital admission and emergency care attendance risk for SARS-CoV-2 Delta (B.1.617.2) compared with Alpha (B.1.1.7) variants of concern: a cohort study, Lancet Infect. Dis. 22 (1) (2022) 35–42. https://doi.org/10.1016/S1473-3099(21)00475-8
[36] J. Wise, et al., Covid-19: Delta variant doubles risk of hospital admission compared with Alpha variant, study shows, BMJ 374 (2021) n2152. News article summarising Twohig et al. Lancet Infect Dis 2021/22 findings. https://doi.org/10.1136/bmj.n2152
[37] T. Nyberg, P. Bager, I.B. Svalgaard, D. Bejko, N. Bundle, J. Evans, T.G. Krause, J. McMenamin, J. Mossong, H. Mutch, et al., A standardised protocol for assessment of relative SARS-CoV-2 variant severity, with application to severity risk for COVID-19 cases infected with Omicron BA. 1 compared to Delta variants in six European countries, arXiv preprint arXiv:2303.05541. (2023).
[38] T. Nyberg, N.M. Ferguson, S.G. Nash, H.H. Webster, et al., Comparative analysis of the risks of hospitalisation and death associated with SARS-CoV-2 Omicron (B.1.1.529) and Delta (B.1.617.2) variants in England: a cohort study, Lancet 399 (10332) (2022) 1303–1312. https://doi.org/10.1016/S0140-6736(22)00462-7
[39] SARS-CoV-2 variants of concern and variants under investigation in England: Technical briefing 31 (Omicron severity update), Technical Report, UK Health Security Agency, 2021. Data cut-off 29 December 2021.
[40] V. Auvigne, et al., Severe hospital events following symptomatic infection with SARS-CoV-2 Omicron and Delta variants in France, EClinicalMedicine 48 (2022) 101455. https://doi.org/10.1016/j.eclinm.2022.101455
[41] V. Andreasen, J. Lin, S.A. Levin, The dynamics of cocirculating influenza strains conferring partial cross-immunity, J. Math. Biol. 35 (7) (1997) 825–842.
[42] J.R. Gog, B.T. Grenfell, Dynamics and selection of many-strain pathogens, Proceed. Natl. Acad. Sci. USA 99 (26) (2002) 17209–17214. https://doi.org/10.1073/pnas.252512799
[43] R. Antia, R.R. Regoes, J.C. Koella, C.T. Bergstrom, The role of evolution in the emergence of infectious diseases, Nature 426 (6967) (2003) 658–661.
[44] G.E. Leventhal, A.L. Hill, M.A. Nowak, S. Bonhoeffer, Evolution and emergence of infectious diseases in theoretical and real-world networks, Nat. Commun. 6 (1) (2015) 1–11.
[45] N.G. Davies, S. Abbott, R.C. Barnard, C.I. Jarvis, A.J. Kucharski, J.D. Munday, C.A.B. Pearson, T.W. Russell, D.C. Tully, A.D. Washburne, et al., Estimated transmissibility and impact of SARS–CoV–2 lineage B.1.1.7 in England, Science 372 (6538) (2021) eabg3055. https://doi.org/10.1126/science.abg3055
[46] E. Volz, S. Mishra, M. Chand, J.C. Barrett, R. Johnson, L. Geidelberg, W. Hinsley, D. Laydon, G. Dabrera, Á. O'Toole, et al., Assessing transmissibility of SARS–CoV–2 lineage B.1.1.7 in England, Nature 593 (7858) (2021) 266–269. https://doi.org/10.1038/s41586-021-03470-x
[47] F. Campbell, B.N. Archer, H. Laurenson-Schafer, Y. Jinnai, F. Konings, N. Batra, B. Pavlin, K. Vandemaele, M.D. Van Kerkhove, T. Jombart, et al., Increased transmissibility and global spread of SARS–CoV–2 variants of concern as at June 2021, Eurosurveillance 26 (24) (2021) 2100509. https://doi.org/10.2807/1560-7917.ES.2021.26.24.2100509
[48] R. Viana, S. Moyo, D.G. Amoako, H. Tegally, C. Scheepers, C.L. Althaus, U.J. Anyaneji, P.A. Bester, M.F. Boni, M. Chand, et al., Rapid epidemic expansion of the SARS–CoV–2 Omicron variant in southern Africa, Nature 603 (7902) (2022) 679–686. https://doi.org/10.1038/s41586-022-04411-y
[49] D. Jiang, Q. Wang, Z. Bai, H. Qi, J. Ma, W. Liu, F. Ding, J. Li, Could the environment affect the mutation of H1N1 influenza virus?, in: Advances in Clinical Immunology, Medical Microbiology, COVID-19, and Big Data, Jenny Stanford Publishing, 2021, pp. 255–267.
[50] H.K. Alexander, T. Day, Risk factors for the evolutionary emergence of pathogens, J. Roy. Soc. Interface 7 (51) (2010) 1455–1474.
[51] M.M. Tanaka, J. Kumm, M.W. Feldman, Coevolution of pathogens and cultural practices: a new look at behavioral heterogeneity in epidemics, Theor. Popul. Biol. 62 (2) (2002) 111–119.
[52] S. Nickbakhsh, C. Mair, L. Matthews, R. Reeve, P.C.D. Johnson, F. Thorburn, B. Von Wissmann, A. Reynolds, J. McMenamin, R.N. Gunson, et al., Virus–virus interactions impact the population dynamics of influenza and the common cold, Proceed. Natl. Acad. Sci. 116 (52) (2019) 27142–27150.
[53] B. Roche, J.M. Drake, P. Rohani, An agent-based model to study the epidemiological and evolutionary dynamics of influenza viruses, BMC Bioinformat. 12 (1) (2011) 87.
[54] B. Roche, P. Rohani, Environmental transmission scrambles coexistence patterns of avian influenza viruses, Epidemics 2 (2) (2010) 92–98.
[55] J. Lourenço, M. Recker, Natural, persistent oscillations in a spatial multi-strain disease system with application to dengue, PLoS Comput. Biol. 9 (10) (2013) e1003308.
[56] S. Bianco, L.B. Shaw, I.B. Schwartz, Epidemics with multistrain interactions: the interplay between cross immunity and antibody-dependent enhancement, Chaos: Interdiscipl. J. Nonlinear Sci. 19 (4) (2009) 043123.
[57] C.J. Browne, A multi-strain virus model with infected cell age structure: application to HIV, Nonlinear Anal. Real World Appl. 22 (2015) 354–372.
[58] J. Mossong, N. Hens, M. Jit, P. Beutels, K. Auranen, R. Mikolajczyk, M. Massari, S. Salmaso, G.S. Tomba, J. Wallinga, J. Heijne, M. Sadkowska-Todys, M. Rosinska, W.J. Edmunds, Social contacts and mixing patterns relevant to the spread of infectious diseases, PLoS Med. 5 (3) (2008) e74. https://doi.org/10.1371/journal.pmed.0050074
[59] E. Zagheni, F.C. Billari, P. Manfredi, M. Möbius, A. Melegaro, J. Mossong, W.J. Edmunds, Using time-use data to parameterize models for the spread of close-contact infectious diseases, Demography 45 (3) (2008) 587–607. https://doi.org/10.1353/dem.0.0017
[60] S.V. Scarpino, A. Allard, L. Hébert-Dufresne, The effect of a prudent adaptive behaviour on disease transmission, Nat Phys 12 (11) (2016) 1042–1046.
[61] L. Fewtrell, R.B. Kaufmann, D. Kay, W. Enanoria, L. Haller, J.M. Colford, Jr, Water, sanitation, and hygiene interventions to reduce diarrhoea in less developed countries: a systematic review and meta-analysis, Lancet Infect. Dis. 5 (1) (2005) 42–52.
[62] C.T. Bauch, D.J.D. Earn, Vaccination and the theory of games, Proceedings of the National Academy of Sciences 101 (36) (2004) 13391–13394.
[63] S. Del Valle, H. Hethcote, J.M. Hyman, C. Castillo-Chavez, Effects of behavioral changes in a smallpox attack model, Math. Biosci. 195 (2) (2005) 228–251.
[64] T. Gross, C.J.D. D'Lima, B. Blasius, Epidemic dynamics on an adaptive network, Phys. Rev. Lett. 96 (20) (2006) 208701.
[65] A. Nold, Heterogeneity in disease-transmission modeling, Math. Biosci. 52 (3–4) (1980) 227–240.
[66] H.W. Hethcote, J.W. Van Ark, Epidemiological models for heterogeneous populations: proportionate mixing, parameter estimation, and immunization programs, Math. Biosci. 84 (1) (1987) 85–118.
[67] R.M. Anderson, R.M. May, Infectious Diseases of Humans: Dynamics and Control, Oxford university press, 1991.
[68] C.R. Williams, A.R. Mikler, Incorporating disgust as disease-avoidant behavior in an agent-based epidemic model, in: International Conference on Social Computing, Behavioral-Cultural Modeling and Prediction and Behavior Representation in Modeling and Simulation, Springer, 2016, pp. 107–116.
[69] M. Oaten, R.J. Stevenson, T.I. Case, Disease avoidance as a functional basis for stigmatization, Philosoph. Transact. Roy. Soc. B: Biolog. Sci. 366 (1583) (2011) 3433–3452.

[70] A. d'Onofrio, P. Manfredi, E. Salinelli, Information-related changes in contact patterns may trigger oscillations in the endemic prevalence of infectious diseases, Theor. Popul. Biol. 71 (3) (2007) 262–270. https://doi.org/10.1016/j.tpb.2006.11.001
[71] M. Ryan, E. Brindal, M. Roberts, R.I. Hickson, A behaviour and disease transmission model: incorporating the health belief model for human behaviour into a simple transmission model, J. Roy. Soc. Interface 21 (215) (2024) 20240038.
[72] O. Diekmann, J.A.P. Heesterbeek, M.G. Roberts, The construction of next-generation matrices for compartmental epidemic models, J. Roy. Soc. Interface 7 (47) (2010) 873–885.
[73] I.N. Lymperopoulos, G.D. Ioannou, Online social contagion modeling through the dynamics of integrate-and-fire neurons, Inf. Sci. (N.Y.) 320 (2015) 26–61.
[74] Z. Cao, Q. Zhang, X. Lu, D. Pfeiffer, Z. Jia, H. Song, D.D. Zeng, Estimating the effective reproduction number of the 2019-nCoV in China, MedRxiv (2020) 01–2020.
[75] B. Tang, X. Wang, Q. Li, N.L. Bragazzi, S. Tang, Y. Xiao, J. Wu, Estimation of the transmission risk of the 2019-nCoV and its implication for public health interventions, J. Clin. Med. 9 (2) (2020) 462.
[76] D. McEvoy, C. McAloon, A. Collins, K. Hunt, F. Butler, A. Byrne, M. Casey-Bryars, A. Barber, J. Griffin, E.A. Lane, et al., Relative infectiousness of asymptomatic SARS-CoV-2 infected persons compared with symptomatic individuals: a rapid scoping review, BMJ Open 11 (5) (2021) e042354.
[77] L. Ferretti, C. Wymant, M. Kendall, L. Zhao, A. Nurtay, L. Abeler-Dörner, M. Parker, D. Bonsall, C. Fraser, Quantifying SARS-CoV-2 transmission suggests epidemic control with digital contact tracing, Science 368 (6491) (2020) eabb6936.
[78] G. Tapiwa, K. Cécile, C. Dongxuan, T. Andrea, F. Christel, W. Jacco, H. Niel, Estimating the generation interval for COVID-19 based on symptom onset data, MedRxiv (2020) 03–2020.
[79] R. Li, S. Pei, B. Chen, Y. Song, T. Zhang, W. Yang, J. Shaman, Substantial undocumented infection facilitates the rapid dissemination of novel coronavirus (SARS-CoV-2), Science 368 (6490) (2020) 489–493.
[80] K.N. Nabi, Forecasting COVID-19 pandemic: a data-driven analysis, Chaos Soliton. Fract. 139 (2020) 110046.
[81] L. Du Plessis, J.T. McCrone, A.E. Zarebski, V. Hill, C. Ruis, B. Gutierrez, J. Raghwani, J. Ashworth, R. Colquhoun, T.R. Connor, et al., Establishment and lineage dynamics of the SARS-CoV-2 epidemic in the UK, Science 371 (6530) (2021) 708–712.
[82] N. Shaikh, P. Swali, R. Houben, Asymptomatic but infectious-The silent driver of pathogen transmission. A pragmatic review. Epidemics 44, 100704, 2023.
[83] S.W. Park, J. Dushoff, B.T. Grenfell, J.S. Weitz, Intermediate levels of asymptomatic transmission can lead to the highest epidemic fatalities, PNAS Nexus 2 (4) (2023) pgad106.
[84] H. Kawasuji, Y. Takegoshi, M. Kaneda, A. Ueno, Y. Miyajima, K. Kawago, Y. Fukui, Y. Yoshida, M. Kimura, H. Yamada, et al., Transmissibility of COVID-19 depends on the viral load around onset in adult and symptomatic patients, PLoS ONE 15 (12) (2020) e0243597.
[85] Z. Guo, G. Xiao, J. Du, W. Cui, B. Li, D. Xiao, A dynamic model for elevator operation-induced spread of a respiratory infectious disease in an apartment building, Heliyon 9 (3) (2023).
[86] A. Andersson-Ellström, L. Forssman, I. Milsom, The relationship between knowledge about sexually transmitted diseases and actual sexual behaviour in a group of teenage girls, Sex. Transm. Infect. 72 (1) (1996) 32–36.
[87] J.N. Hays, Epidemics and Pandemics: their Impacts on Human History, Abc-clio, 2005.
[88] V.A. Curtis, Infection-avoidance behaviour in humans and other animals, Trend. Immunol. 35 (10) (2014) 457–464.
[89] A. Azizi, C. Kazanci, N.L. Komarova, D. Wodarz, Effect of human behavior on the evolution of viral strains during an epidemic, Bull. Math. Biol. 84 (12) (2022) 144.
[90] C. Eksin, J.S. Shamma, J.S. Weitz, Disease dynamics in a stochastic network game: a little empathy goes a long way in averting outbreaks, Sci. Rep. 7 (1) (2017) 1–13.
[91] C. Eksin, K. Paarporn, J.S. Weitz, Systematic biases in disease forecasting–the role of behavior change, Epidemics 27 (2019) 96–105.
[92] J.S. Weitz, S.W. Park, C. Eksin, J. Dushoff, Awareness-driven behavior changes can shift the shape of epidemics away from peaks and toward plateaus, shoulders, and oscillations, Proceed. Natl. Acad. Sci. 117 (51) (2020) 32764–32771.